Electromagnetic Force Modification in Fault Current Limiters under Short-Circuit Condition Using Distributed Winding Configuration

Asef Ghabeli*[1] and Mohammad Reza Besmi†[1]

[1]Faculty of Engineering, Shahed University, Tehran, Iran

May 21, 2016

Abstract

The electromagnetic forces caused by short-circuits consisting of radial and axial forces impose mechanical damages and failures to the windings. The engineers have tried to decrease these forces using different techniques and innovations. Utilization of various kinds of winding arrangements is one of these methods, which enable the transformers and fault current limiters to tolerate higher forces without a substantial increase in construction and fabrication costs. In this paper, a distributed winding arrangement is investigated in terms of axial and radial forces during short-circuit condition in a three-phase FCL. To calculate the force magnitudes of AC and DC supplied windings, a model based on the finite element method in time stepping procedure is employed. The three-phase AC and DC supplied windings are split into multiple sections for more accuracy in calculating the forces. The simulation results are compared with a conventional winding arrangement in terms of leakage flux and radial and axial force magnitudes. The comparisons show that the distributed winding arrangement mitigates radial and especially axial force magnitudes significantly.

Keywords : Fault Current Limiter, Short-circuit Current, Finite Element Method, Electromagnetic Force.

1 Introduction

Due to extending power grids and increasing number of loads in power systems, the amount of power delivery and so on the magnitude of fault currents will be increased. Therefore, the rated currents of circuit breakers should be increased to deal with such faults which are not economic [1–4]. Fault

*asefghabeli@gmail.com
†besmi@shahed.ac.ir

current limiters (FCL) will solve the aforementioned problems by limiting the fault currents to an acceptable limit. Thus, the expensive equipments and upgrades would not be necessary. FCLs are installed in series with electric lines. During normal conditions, FCL impedance is very small, but when a fault happens, it increases and limits the high current of the fault. Short-circuits generate high current conditions in FCL windings. These currents induce excessive forces in FCL windings which may cause axial or radial bending, buckling and hooping stresses and etc. Consequently, electromagnetic forces in the FCL windings are important considerations in the design, manufacturing and operation of FCLs [5].

Before installing FCL on electric power system, the maximum electromagnetic force due to short-circuit current should be predicted for safe operation. Any kind of deficiency in the winding structure strength due to miscalculation may cause to mechanical collapse and permanent deformation of windings. However, it is not easy to predict the transient electromagnetic force accurately, because of the complicated structure of FCL windings [3, 4, 6]. In recent years, many studies have been done around electromagnetic force calculation caused by short-circuits in different types of transformers and FCLs. In Ref. [7], a study was carried out to investigate the effectiveness of finite element analysis to calculate the forces applied on the windings of a single-phase shell-type transformer. Also, the sensitivity of these methods explored to the very small changes in configuration. Then, suitability of 2-D or 3-D analysis with consideration of skin and proximity effects and their effects on the force distribution was studied. In Ref. [8], 3-D computations on a single-phase shell-type power transformer using the Hopfield neural network energy minimization technique have been done. Afterwards, the forces resulting from inrush and short-circuit current have been compared. In Ref. [9], a 720-MVA power transformer was simulated and by means of a 3-D A-V-A coupled formulation, the eddy current field and the electric circuit equations were solved simultaneously. In addition, axial, radial and the torsional forces acting on the spiral coils were computed and the capability of the coils to tolerate these forces were investigated. A 70 MVA three-phase split-winding transformer, under preset and postset short-circuit test conditions was simulated with a 2-D nonlinear-transient finite element model, and the results were compared and verified by a 3-D model in Ref. [10]. In Ref. [11], a three-phase three-legged core-type power transformer has been modeled in 2-D and 3-D. The electromagnetic forces due to short-circuit and inrush current using finite element method have been calculated and compared, taking into account the asymmetry of phase current in the inrush current condition. In Ref. [12], the experimental verification and finite element analysis of electromagnetic force caused by short-circuit for a dry-type transformer has been done. The simulation data were used to predict stress distributions or deformations of windings. In Ref. [13], a study has been presented for calculation of mechanical force in the windings of a high-current HTS transformer with two auxiliary windings. The calculations have been done using finite-element method considering non-uniformity of both field and current distributions. The study has shown that unbalancing current distribution may increase the mechanical forces in the windings. Also an exact model for calculation of mechanical force in the windings with aforementioned conditions has been developed. In Ref. [14], Aracil et. al. compared the effects of electromagnetic forces in superconducting FCL (SFCL) and a typical power transformer coils using boundary element method. They found that there are considerable differences between the force distributions in them that have to be considered

during the design process.

In this paper, finite element analysis is used to calculate the electromagnetic forces on the windings of a pre-designed scaled-down lab inductive FCL. First, the magnetic flux density in the FCL in normal and short-circuit conditions has been calculated. Afterwards, the axial and radial electromagnetic forces in each section of the DC and AC supplied windings, for two different types of winding arrangements in transient condition has been calculated. In the first winding arrangement, phase windings are placed one next to each other and in the second one, a winding turn of one phase is placed between the winding turns of two other phases. Finally the radial and axial forces in these two types of winding arrangements have been compared.

2 Finite Element Analysis

2.1 An Overview of the Method

FEM is a complicated tool which can be used by engineers, scientists and researchers to solve any kind of engineering problem. This method is a pioneer numerical analysis method among the other numerical ones, for simulation of physical field distributions, which has the capability of solving the problems independently of other methods. All the requirements for FEM to solve a problem, is a finite set of spatial partial derivative equations, appropriate boundary and initial conditions. With these, FEM can solve all kinds of static, steady state and transient engineering problems [15–17].

By solving Maxwell equation in a finite region of space, with appropriate boundary condition and sometimes if necessary, with initial conditions defined by user to ensure that the solution is unique, FEM can be able to solve any kind of electromagnetic field problems. To solve, the problem geometry is divided into tetrahedral or triangular elements called mesh. Each of these elements gives a quadratic polynomial that represents the unknown characteristics of field being calculated. By solving these equations, the unknown characteristics of field can be solved in the whole geometry [18–20].

To analyze using finite element, the 2-Dimensional (2-D), double 2-Dimensional (double 2-D), or three-Dimensional (3-D) simulations can be used. The 2-D approach is useful for simulation of inrush current, external short-circuit, and major internal short-circuit, because it is faster than the 3-D approach. However, this kind of simulation is not appropriate for instance, loss calculation of transformer under non-sinusoidal voltage, because in 2-D simulation, the depth of geometry is not considered and the parameters of transformer are not accurate enough. After all, the 3-D simulations are more accurate than 2-D simulations [21].

2.2 Basic Equations

The electromagnetic forces are calculated through the local magnetic flux density of the windings in the FCL. One of the numerical methods, finite element analysis is used for calculating the leakage flux in the winding region [11, 12]. Considering a known current density and neglecting the electric

field, the magnetic field intensity vector, can be obtained from equation below:

$$\nabla \times \overrightarrow{H} = \overrightarrow{J} \tag{1}$$

Then, the magnetic flux density can be obtained from this equation:

$$\overrightarrow{B} = \mu_0 \mu_r \overrightarrow{H} \tag{2}$$

Where μ_0 and μ_r are the space permeability and relative permeability, respectively. An auxiliary vector called magnetic potential vector, $\overrightarrow{A}$ is used to save computation time which obtained as below:

$$\nabla \times \overrightarrow{A} = \overrightarrow{B} \tag{3}$$

When source current density (J) flows in the windings of FCL, using equations (1) to (3), the equation of magnetic field is given as below:

$$\nabla \times \frac{1}{\mu_0 \mu_r} (\nabla \times \overrightarrow{A}) = \overrightarrow{j} \tag{4}$$

The magnetic vector potential computed by magnetic field analysis is used for calculation of magnetic flux density and electromagnetic forces in the winding of FCL.

2.3 Transient Currents

The magnitude of transient current would be an important factor for calculation of electromagnetic force in the FCL windings. The inductive FCL investigated in this paper, is based on core saturation effect. The FCL only has the capability of limiting single-phase-to-ground faults. This type of fault occurs when one phase is short-circuited to ground, which might be happens due to lightning strikes, debris, pollution effects, animals and vegetations [5].

The short-circuit current is inversely proportional with sum of transformer impedance and system impedance. In a single phase transformer, the short-circuit current at transient condition can be approximately expressed as follows [6].

$$I_{sc}(t) = I_0 e^{(-\frac{R}{L}t)} + \frac{V_m}{\sqrt{(R^2 + X^2)}} \cos \omega t \tag{5}$$

Where I_{sc} is short-circuit current [A], I_0 is initial current [A], R, L and X are resistance [Ω], inductance [H], and reactance [Ω], respectively, and V_m is maximum voltage [V].

The electrical circuit that has been used in simulation for initiating the fault consisted of a three-phase transformer which supplies a line-to-line voltage of 65 V_{rms} connected to a three-phase resistive load with resistance of 11 Ω via the FCL. For initiating the fault, the load resistor in phase c was short-circuited at 4^{th} second. This moment has been chosen to make sure that the FCL is in steady state condition and the DC supplied windings have completely driven the two FCL core legs into saturation. The fault caused a maximum current of 395 passed through the FCL AC supplied windings at its first cycle. The electrical circuit used for fault inception, coupled with magnetic model of simulated FCL, has been shown in Figure 1.

The parameters of fault inception circuit are summarized in table 1.

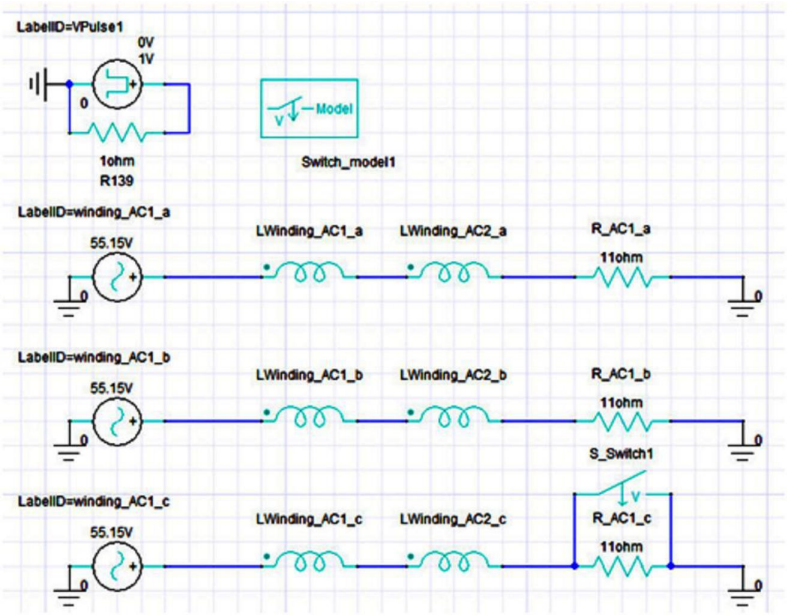

Figure 1: Electrical circuit coupled with magnetic model of simulated FCL for fault inception

Table 1: Fault inception circuit parameters

Parameters	Value
Line-to-line voltage [V_{rms}]	65
Fault current amplitude [A_{rms}]	395
Load resistance [Ω]	11
DC current [A]	10

2.4 Electromagnetic Forces

The current that is carrying by conductors of the FCL windings are situated in the magnetic leakage field. By the fundamental principle of electromagnetic, these conductors will be exposed to a force due to the interaction between the electric and magnetic fields. This electromagnetic force is calculated as the vector product of current density and magnetic field density as given in equation below [5, 12, 22]:

$$F = J \times B \tag{6}$$

Where F, J and B are force [N], current density [A/m^2] and magnetic flux density [T], respectively.

Short-circuit current will effect on both flux density B and current density J in equation (6).

This means that, force is proportional to the square of current. The direction of the forces is certified by the vector product in equation (6), indicating that the force will act perpendicular to the plane formed by the magnetic field density and current direction [5, 22].

Electromagnetic forces in FCL windings can be subdivided into axial and radial forces. Axial forces occur in a direction parallel to the winding height. Due to the pattern of the magnetic leakage field, the windings experience opposing forces at the winding ends, leading to compressive forces. The highest bending of the magnetic field occurs at the winding ends, consequently maximum axial force is generated there [5, 21]. Radial forces occur perpendicular to the winding height. This kind of force occurs in almost all parts of winding, where the flux lines are parallel to the winding. Its direction depends on the direction of current flowing, therefore the force can result in a compressive or tensile stress.

3 Modeling of Simulated FCL

In this paper, a pre-designed scaled-down lab FCL with two different winding arrangements has been modeled in 2-D. This FCL is a three phase inductive FCL with a common core that operates based on core saturation effect. Figure 2 shows the modeled FCL with two different winding arrangements.

It can be seen from Figure 2 that each of the two outer legs contains one winding of each phase. Blue, red, and green colors denote the windings of phases a, b, and c, respectively. Each phase winding has 9 turns and the AC supplied windings from the same phase are connected in series. One DC supplied winding with 40 turns, marked with black colors is placed on each outer leg which also connected in series. In Figure 2(a) the conventional winding arrangement for FCL with the phase windings next to each other has been shown. In Figure 2(b) the distributed winding arrangement has been shown. It can be seen that the phase windings are wound simultaneously, so that a winding turn of one phase is placed between the winding turns of two other phases. This arrangement results in better magnetic coupling and consequently less leakage flux.

The Specifications and dimensions of the modeled FCL are shown in table 2 and table 3, respectively.

Table 2: Modeled FCL Specifications

Classification	Value
Core material	Grain-oriented silicon-steel sheets
Typical magnetic field intensity saturation level [A/m]	800
Typical magnetic flux density saturation level [T]	1.84
Number of DC turn per leg	40
Number of AC turns per phase and per leg	125

The DC and AC supplied windings were divided into 10 and 9 sections, respectively, for computation of electromagnetic force. With this modeling technique, it is possible to calculate the

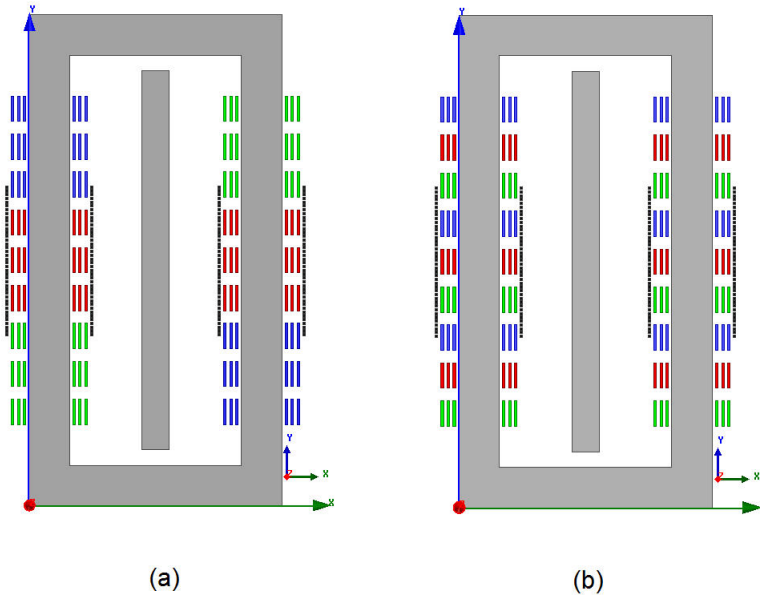

Figure 2: The modeled three-phase single-core FCL with the (a) phase windings placed one next to each other (Conventional) (b) Distributed phase windings. The blue, red and green colors show phase a, b, and c, respectively.

Table 3: Modeled FCL Dimensions

Parameter	Value
Cross-section of outer leg $[m^2]$	13.5×10^{-4}
Cross-section of middle leg $[m^2]$	9×10^{-4}
Core width [m]	0.2
Core height [m]	0.41
Core depth [m]	0.042
Window width [m]	0.155
Window height [m]	0.325
Width of middle leg [m]	0.03
Gap Length [m]	2×0.0125

electromagnetic forces on any particular positions (or parts) of windings and anticipate mechanical stress and probable deformations and hazards, because of too much forces exerted on the windings. The greater number of sections leads to more accurate results. Therefore, by performing required

consideration in design and manufacturing, the aforementioned deformations and damages can be avoided [22].

4 Result and Discussion

4.1 Simulation Results

The magnetic vector potential computed by magnetic field analysis is used for calculation of magnetic flux density and electromagnetic forces in the FCL windings. In this paper, the parameters are processed using Maxwell v.14 based on finite element method. The simulations are processed and solved in transient solution type. The total number of mesh elements is 6340 and the calculation time for each simulation is about 30 minutes. Figure 3 shows the meshed FCL.

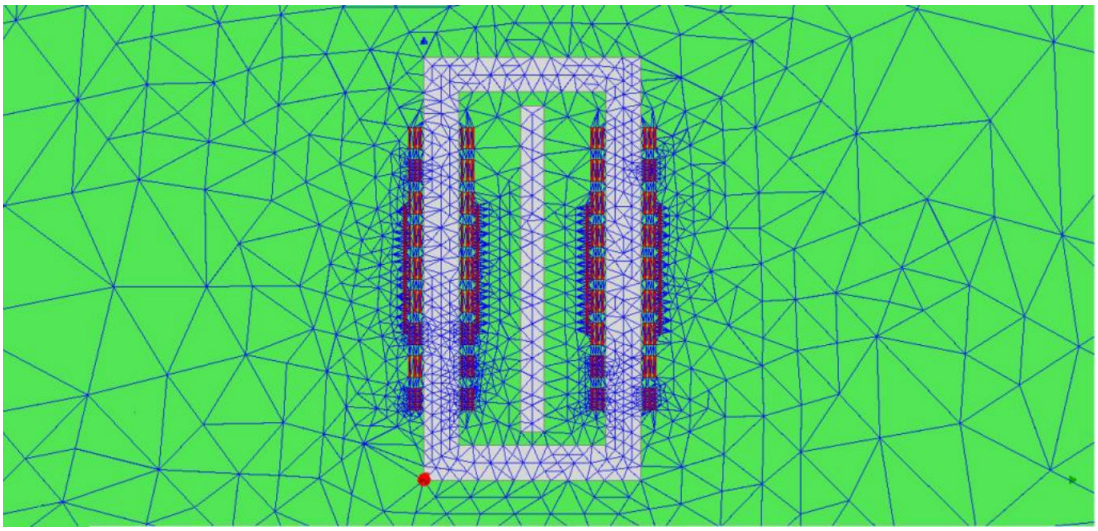

Figure 3: The meshed FCL

Figure 4 shows the distribution of magnetic flux density for FCL with the conventional winding arrangement (depicted in Figure 2(a)). In Figure 4(a) and 4(b) the magnetic flux distribution in normal and short-circuit condition are shown, respectively. Figure 5 shows the distribution of magnetic flux density for FCL with the distributed winding arrangement (depicted in Figure 2(b)). In Figures 5(a) and 5(b) the magnetic flux distribution in normal and short-circuit condition are shown, respectively. As it can be seen in these figures, in one half cycle, the short-circuit current drives one of the legs deeper into saturation while drives the other leg out of saturation, and this process is repeated alternatively in each half cycle. In Figures 4(b) and 5(b) the leakage flux densities around short-circuited windings due to the high currents of short-circuit can be seen.

Interactions between these leakage fluxes and high currents cause high magnitude electromagnetic forces.

Figures 4(a) and 5(a) depict that the core saturates in steady state and the magnetic flux density is distributed uniformly over the core in normal condition. In Figure 4(b), when short-circuit occurs, the flux lines accumulate in a region and drive that region fully into saturation, which leads to maximum flux density of 2.56 T. But as it can be seen in Figure 5(b) for distributed winding arrangement and during short-circuit condition, the flux lines scatter all over the core which leads to less maximum flux density, about 2.46 T. This happens because of the particular arrangement of winding which each turn of one phase is placed in between two turns of other phases. Less maximum flux density leads to less saturation and finally less leakage flux and less maximum electromagnetic force compared to the conventional winding arrangement.

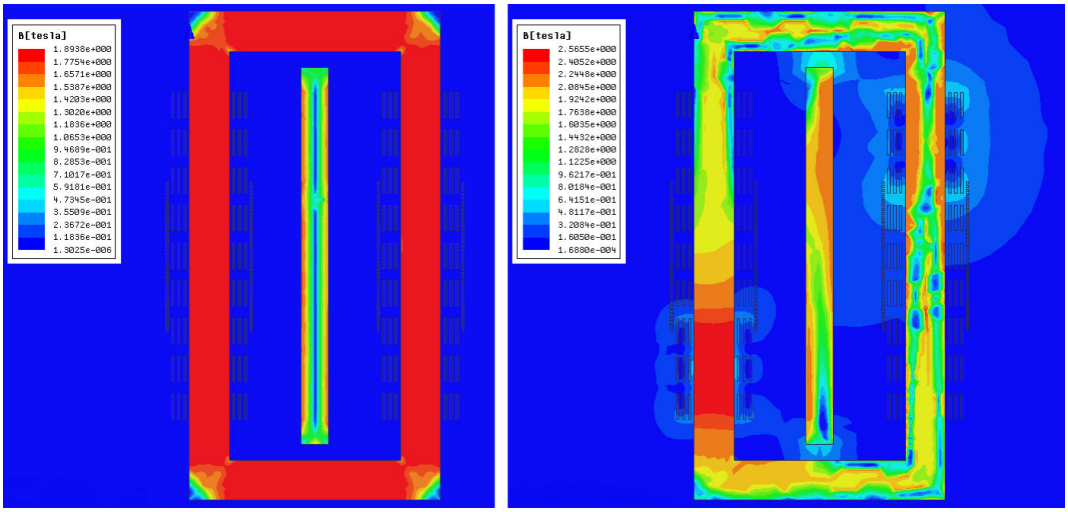

Figure 4: Distribution of magnetic flux density for FCL with conventional windings (a) Saturation mode before fault (b) 20 ms after fault

4.2 Electromagnetic Force Calculations

The electromagnetic forces including radial and axial forces were calculated for AC and DC supplied windings of FCL accurately, using transient solution type. The exact values of maximum electromagnetic forces for each 10 and 9 sections of DC and AC supplied windings, respectively, have been obtained during a cycle after the fault inception on phase winding c.

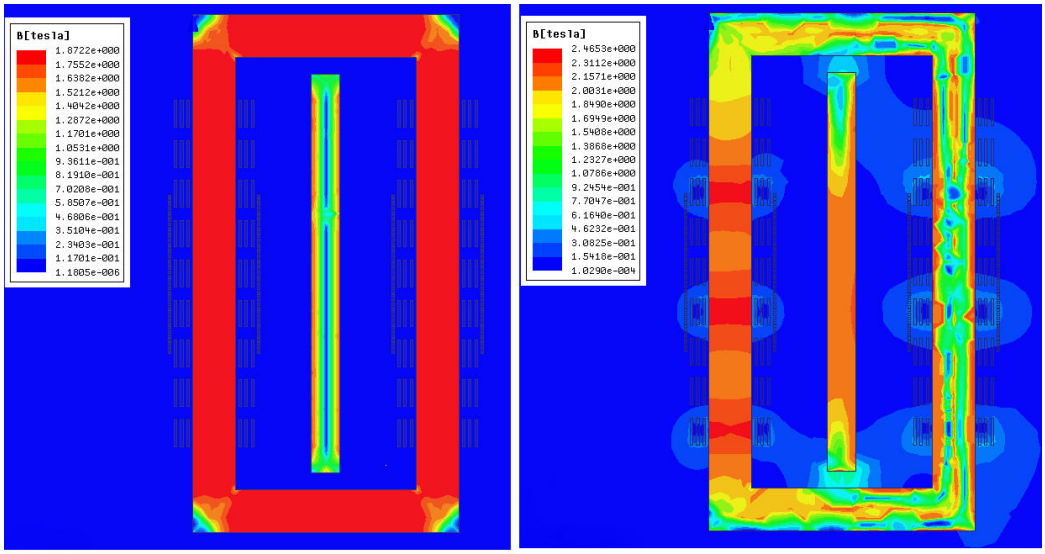

Figure 5: Distribution of magnetic flux density for FCL with distributed windings (a) Saturation mode before fault (b) 20 ms after fault

4.2.1 Conventional Winding Arrangement

In table 4 and table 5, the radial and axial force magnitudes and force magnitude for the conventional winding arrangement and for each section of AC and DC supplied windings, are shown, respectively.

As it can be seen in table 4, the radial and axial forces in short-circuit mode in phase winding c has a considerable magnitude and increased hundred times compared to the normal condition. These forces in other two phases did not change significantly in compared to phase c. In the case of DC supplied windings, the forces did not change significantly compared to normal condition, unless for the sections of DC supplied windings which were exposed to intense leakage fluxes caused by short-circuited winding c , as it can be seen in Figure 6. In these sections of DC supplied windings, the axial and radial forces increased about a hundred times than normal condition.

4.2.2 Distributed winding arrangement

After the short-circuit, the electromagnetic forces including radial and axial forces were also calculated for each section of AC and DC supplied windings of the distributed winding arrangement and the results were shown in table 6 and table 7, respectively.

As the previous winding arrangement, it can be seen that the radial and axial forces in

Table 4: Radial and axial forces and force magnitude in each section of AC supplied windings for the conventional winding arrangement

Phase	Section	Radial Force Magnitude	Axial Force Magnitude	Force Magnitude
a	1	0.24	1.54	1.56
	2	0.26	1.7	1.72
	3	0.29	1.95	1.97
b	4	2.7	6.63	7.16
	5	2.76	12.523	12.84
	6	1.03	23.53	23.55
c	7	94.947	174.5	198.71
	8	109.48	3.145	109.52
	9	95.65	181.26	204.95

Table 5: Radial and axial forces and force magnitude in each section of DC supplied winding for the conventional winding arrangement

Section	Radial Force Magnitude	Axial Force Magnitude	Force Magnitude
1	0.6	5.96	6
2	0.84	6.6	6.68
3	1	7.72	7.76
4	0.72	9	9.04
5	0.56	10.52	10.56
6	0.12	12.72	12.72
7	1.48	15.32	15.4
8	4.04	19.48	19.56
9	9.72	23.72	25.64
10	24.6	21.2	23.48

short-circuit mode in phase winding c have considerable values in comparison to its normal condition and two other phases. Table 6 and Figure 7 show that the DC supplied windings of the distributed winding arrangement follow the same rules and interpretations that have been illustrated for the conventional winding arrangement. For example, for DC supplied winding, sections 7, 8, 9 have more radial forces compared to those which are not exposed to the intense leakage flux caused by short-circuited winding c [22].

Accordingly, it can be concluded that the axial and radial forces in DC supplied winding depend on the winding arrangement, the phase which short-circuit occurs, and more importantly, situation of DC supplied winding with respect to the short-circuited phase.

Figures 8 and 9 depict the maximum electromagnetic forces for AC and DC supplied windings of the simulated FCL in a cycle after the fault, for two types of winding arrangements, respectively. It ought to be noted that the average forces of AC supplied windings are calculated for short-circuited

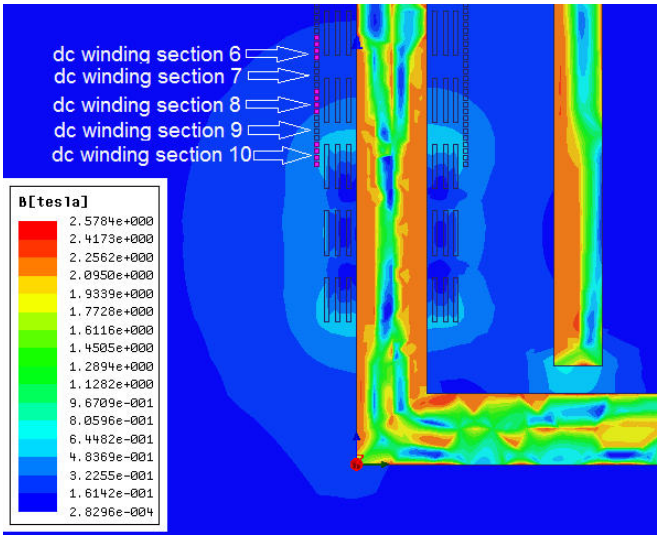

Figure 6: Sections of DC supplied winding surrounded by leakage fluxes caused by phase winding c for the conventional winding arrangement

Table 6: The magnitude of radial and axial forces and force magnitude in each section of AC supplied windings for the distributed winding arrangement

Phase	Section	Radial Force Magnitude	Axial Force Magnitude	Force Magnitude
a	1	0.16	2.42	2.43
	4	0.19	0.72	0.75
	7	0.22	1.81	1.82
b	5	1.46	23.96	24
	5	1.02	12.52	12.56
	8	1.52	7.62	7.77
c	3	75.843	49.28	9.449
	6	75.265	0.525	75.267
	9	77.117	55.87	95.239

phase c. Comparing forces of two winding arrangements, it can be derived that for short-circuited winding of distributed winding arrangement, the maximum radial and axial forces had about 24% and 70% decrease in magnitude, respectively, with respect to the conventional winding arrangement.

It is very important to note that, all of the force magnitudes listed in the above tables are related

Table 7: The magnitude of radial and axial forces and force magnitude in each section of DC supplied winding for the distributed winding arrangement

Section	Radial Force Magnitude	Axial Force Magnitude	Force Magnitude
1	19.64	2.6	18.76
2	7.12	5.92	9.24
3	3.8	2.24	4.44
4	2.48	1.12	2.72
5	2.72	4.56	5.32
6	5.48	8.6	10.12
7	13.32	10.56	17
8	22.32	0.64	22.32
9	12.12	11.08	16.44
10	5.52	8.4	10.04

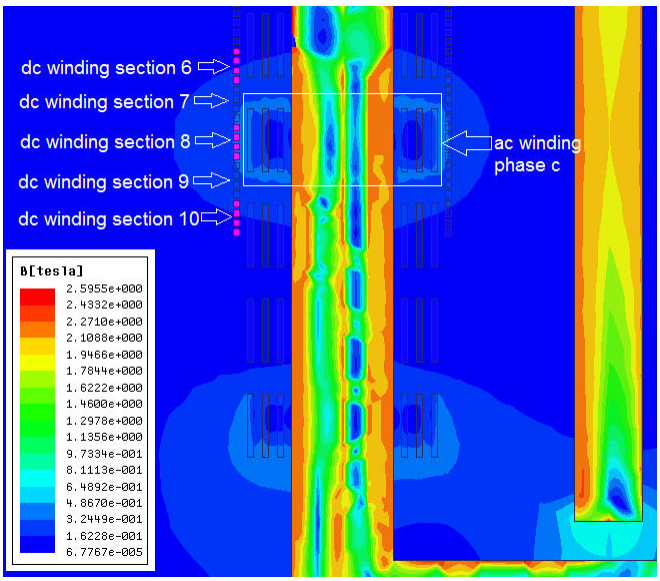

Figure 7: Sections of DC supplied winding surrounded by leakage fluxes caused by phase winding c for the distributed winding arrangement

to a scaled-down lab FCL with very smaller dimensions, rated power and also rated short-circuit current than industrial ones in a real power network. In industrial dimensions, the short-circuit currents are hundreds or even thousands times bigger, therefore the forces are much greater than

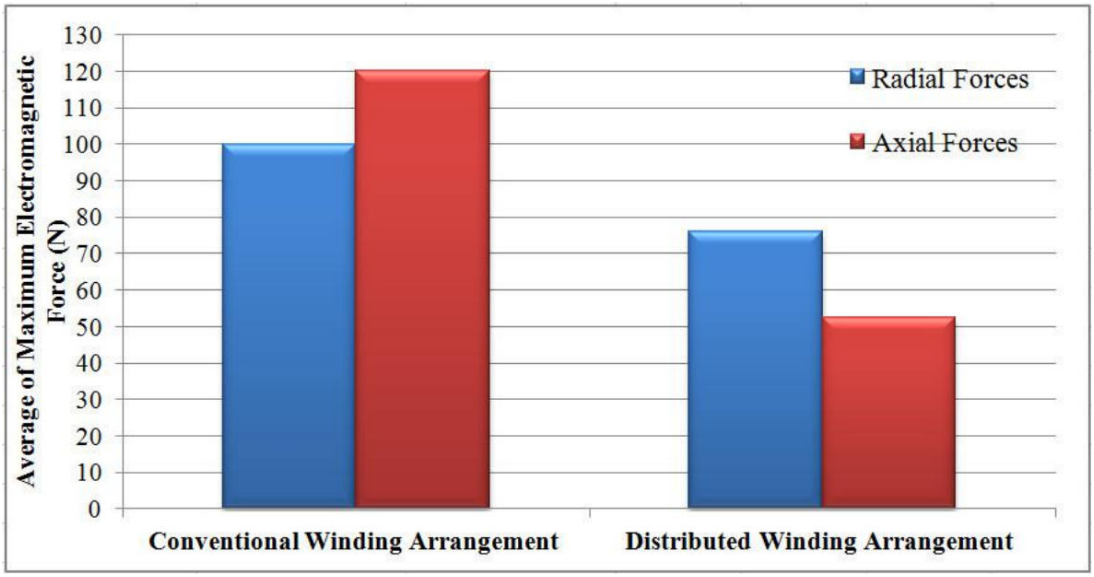

Figure 8: Average of maximum electromagnetic forces of AC supplied windings for simulated FCL

the values calculated in this paper. In all, the values in this paper are mentioned only for the purpose of comparison to the other winding arrangement and are not a real value in a real power network.

5 Conclusion

In this paper, distributed winding arrangement is investigated in terms of axial and radial forces during short-circuit condition in a three-phase FCL. To calculate the axial and radial forces of the FCL, 2-Dimensional FCL model is analyzed using the finite element method. The short-circuit current with a magnitude of 395 A is applied to phase winding c, and axial and radial forces of DC and AC supplied windings are calculated in transient state. For comparison purposes, these forces is compared with forces obtained from simulation results of a conventional winding arrangement which the phase windings are placed one next to each other. The comparison showed that the distributed winding arrangement has mitigated the average radial and axial forces about 24% and 70%, respectively, in short-circuit condition. These considerable decreases in forces were obtained only with modifying the arrangement of winding and with minimum value of cost. This fact makes the distributed winding arrangement an appropriate choice for FCL devices.

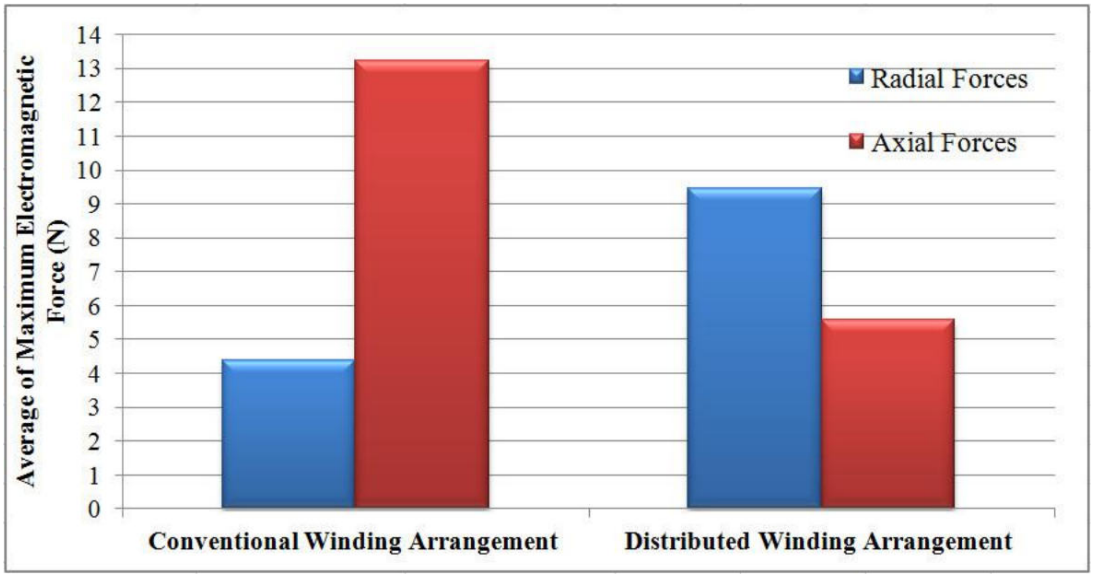

Figure 9: Average of maximum electromagnetic forces of DC supplied windings for simulated FCL

References

[1] S. S. Kalsi and A. Malozemoff, "Hts fault current limiter concept," in *Power Engineering Society General Meeting, 2004. IEEE.* IEEE, 2004, pp. 1426–1430.

[2] Y. Xin, W. Gong, X. Niu, Z. Cao, J. Zhang, B. Tian, H. Xi, Y. Wang, H. Hong, Y. Zhang *et al.*, "Development of saturated iron core hts fault current limiters," *Applied Superconductivity, IEEE Transactions on*, vol. 17, no. 2, pp. 1760–1763, 2007.

[3] A. Rahman, M. Azizi, T. Lie, and K. Prasad, "Computation of the thermal effects of short circuit currents on hts transformer windings," *Applied Superconductivity, IEEE Transactions on*, vol. 22, no. 6, pp. 5 501 211–5 501 211, 2012.

[4] ——, "The effects of short-circuit and inrush currents on hts transformer windings," *Applied Superconductivity, IEEE Transactions on*, vol. 22, no. 2, pp. 5 500 108–5 500 108, 2012.

[5] A. Ghabeli, M. Yazdani-Asrami, and S. A. Gholamian, "A novel unsymmetrical multi-segment concentric winding scheme for electromagnetic force and leakage flux mitigation in hts power transformers," *Applied Superconductivity, IEEE Transactions on*, vol. 25, no. 6, pp. 1–10, 2015.

[6] G. P. Peter, "Calculations for short circuit withstand capability of a distribution transformer," *International Journal of Advancements in Technology*, vol. 2, no. 1, pp. 142–150, 2011.

[7] S. Salon, B. LaMattina, and K. Sivasubramaniam, "Comparison of assumptions in computation of short circuit forces in transformers," *Magnetics, IEEE Transactions on*, vol. 36, no. 5, pp. 3521–3523, 2000.

[8] A. Adly, "Computation of inrush current forces on transformer windings," *Magnetics, IEEE Transactions on*, vol. 37, no. 4, pp. 2855–2857, 2001.

[9] S. Ho, Y. Li, H.-c. C. Wong, S. Wang, and R. Tang, "Numerical simulation of transient force and eddy current loss in a 720-mva power transformer," *Magnetics, IEEE Transactions on*, vol. 40, no. 2, pp. 687–690, 2004.

[10] G. Kumbhar and S. Kulkarni, "Analysis of short-circuit performance of split-winding transformer using coupled field-circuit approach," *Power Delivery, IEEE Transactions on*, vol. 22, no. 2, pp. 936–943, 2007.

[11] J. Faiz, B. M. Ebrahimi, and T. Noori, "Three-and two-dimensional finite-element computation of inrush current and short-circuit electromagnetic forces on windings of a three-phase core-type power transformer," *Magnetics, IEEE Transactions on*, vol. 44, no. 5, pp. 590–597, 2008.

[12] H.-M. Ahn, J.-Y. Lee, J.-K. Kim, Y.-H. Oh, S.-Y. Jung, and S.-C. Hahn, "Finite-element analysis of short-circuit electromagnetic force in power transformer," *Industry Applications, IEEE Transactions on*, vol. 47, no. 3, pp. 1267–1272, 2011.

[13] H. Heydari and F. Faghihi, "Mechanical force analysis in heavy-current hts transformers based on field and current nonuniformity coupled analysis," *Applied Superconductivity, IEEE Transactions on*, vol. 20, no. 4, pp. 2276–2282, 2010.

[14] J. C. Aracil, J. Lopez-Roldan, J. C. Coetzee, F. Darmann, and T. Tang, "Analysis of electromagnetic forces in high voltage superconducting fault current limiters with saturated core," *International Journal of Electrical Power & Energy Systems*, vol. 43, no. 1, pp. 1087–1093, 2012.

[15] M. N. Sadiku, *Numerical techniques in electromagnetics with MATLAB*. CRC press, 2011.

[16] G.-R. Liu and S. S. Quek, *The finite element method: a practical course*. Butterworth-Heinemann, 2013.

[17] J. Chaskalovic, "Mathematical and numerical methods for partial differential equations," 2013.

[18] J.-M. Jin, *The finite element method in electromagnetics*. John Wiley & Sons, 2014.

[19] A. Ghabeli, M. Yazdani-Asrami, M. Besmi, and S. A. Gholamian, "Optimization of distributive ratios of apportioned winding configuration in hts power transformers for hysteresis loss and leakage flux reduction," *Journal of Superconductivity and Novel Magnetism*, vol. 28, no. 12, pp. 3463–3479, 2015.

[20] M. R. Feyzi and M. Sabahi, "Finite element analyses of short circuit forces in power transformers with asymmetric conditions," in *Industrial Electronics, 2008. ISIE 2008. IEEE International Symposium on*. IEEE, 2008, pp. 576–581.

[21] A. G. Juybari and M. R. Besmi, "Calculation of ac loss for high temperature superconductor transformers using two-dimensional finite element method."

[22] H.-M. Ahn, Y.-H. Oh, J.-K. Kim, J.-S. Song, and S.-C. Hahn, "Experimental verification and finite element analysis of short-circuit electromagnetic force for dry-type transformer," *Magnetics, IEEE Transactions on*, vol. 48, no. 2, pp. 819–822, 2012.